# PCCP

## Accepted Manuscript

This is an *Accepted Manuscript*, which has been through the Royal Society of Chemistry peer review process and has been accepted for publication.

*Accepted Manuscripts* are published online shortly after acceptance, before technical editing, formatting and proof reading. Using this free service, authors can make their results available to the community, in citable form, before we publish the edited article. We will replace this *Accepted Manuscript* with the edited and formatted *Advance Article* as soon as it is available.

You can find more information about *Accepted Manuscripts* in the **Information for Authors**.

ARTICLE TYPE

# Rayleigh Light Scattering Properties of Atmospheric Molecular Clusters Consisting of Sulfuric Acid and Bases†

**Jonas Elm,**[*a] **Patrick Norman,**[b] **and Kurt V. Mikkelsen**[a]

The Rayleigh light scattering properties of $(H_2SO_4)_a(NH_3)_b$ and $(H_2SO_4)_a((CH_3)_2NH)_b$ atmospheric molecular clusters have been investigated using a response theory approach. Using density functional theory the molecular structures and stepwise formation free energies for clusters with $a$ and $b$ up to 4 have been re-investigated. The Rayleigh scattering intensities are calculated from the dipole polarizability tensor $\alpha$ using the CAM-B3LYP functional by applying linear response methods. The intrinsic scattering properties of the $(H_2SO_4)_a(NH_3)_b$ and $(H_2SO_4)_a((CH_3)_2NH)_b$ indicate that amine containing clusters scatter light significantly more efficiently then their ammonia containing counterparts. Using the Atmospheric Cluster Dynamics Code (ACDC) the steady state cluster concentrations are estimated and the effective scattering is calculated. The effective scattering is shown to be highly dependent on the estimated concentrations and indicates that there exist competitive pathways, such as nucleation and coagulation, which influences the cluster distributions. The frequency dependence of the scattering is found to depend on the cluster composition and show increased responses when clusters contain more bases than acid molecules. Based on structures obtained using semi-empirical molecular dynamics simulations the Rayleigh scattering properties of clusters with up to 20 acid-base pairs are evaluated. This study represents the first step towards gaining a fundamental understanding of the scattering properties of small atmospheric clusters in the ambient atmosphere.

## 1 - Introduction

The uncertainties related to atmospheric aerosols is the largest issue concerning current climate estimation and prediction for the future. Aerosols affect the global climate directly by scattering the incident light from the sun[1]. Two types of scattering events are possible: either elastic or inelastic. For molecules, clusters and small particles with diameters much smaller than the wavelength of the light, Rayleigh scattering is the principle type of elastic scattering. The inelastic counterpart corresponds to Stokes Raman scattering, where the wavelength of the scattering light is reduced in the process. While the Rayleigh scattering properties of large aerosol particles are relatively well known, the scattering properties of molecular clusters are still not covered, nor understood at the molecular level. Molecular pre-nucleation clusters are omnipresent in the atmosphere, with reported concentration values in the range of 100-100,000 cm$^{-3}$[2–4]. While some of these clusters are able to grow to larger sizes, a significant fraction exists as a background pool. Currently, very little is known about the direct atmospheric impact of these clusters and due to the high concentrations the Rayleigh light scattering properties of this background pool of molecular clusters might not be negligible. These pre-nucleation clusters are likely to be linked to subsequent nucleation events, and the formation of new particles from the background pool is still an unresolved issue. While nucleation is currently believed to occur via the formation of small molecular clusters, very little is known about the exact mechanisms[5]. It has been well established that sulfuric acid is a key component, but formation of new particles cannot be explained without an additional stabilizer. The most commonly proposed stabilizers are ammonia[6–12], amines[13–19] and highly oxidized organic compounds[20–36]. It was recently shown by Almeida *et al.* that dimethylamine above three parts per trillion by volume (PPTV) was able to enhance new particle formation rates by more than 1,000-fold compared to ammonia[37]. This enhancement is attributed to a base-stabilization mechanism involving the formation of sulfuric acid-amine pairs, which strongly decrease the evaporation rate. In a recent study by Kürten *et al.* it was demonstrated that clusters containing 2 sulfuric acid molecules and 1-2 dimethylamine molecules is sufficiently stable, and not susceptible to evaporation[38]. The formation of new particles by stabilization of highly oxidized organic compounds, is still not understood, but is believed to involve 1-4 oxidized

---

organic compounds and 1-3 sulfuric acid molecules[39]. Since the molecular interaction between ammonia/amines and sulfuric acid have been extensively investigated, we here wish to investigate the Rayleigh light scattering properties of these systems. Recently, we reported the necessary tools for studying the Rayleigh light scattering properties of molecular clusters using a bottom-up quantum mechanical response theory approach[40]. This approach makes it possible to investigate non-spherical particles. From simulations of $(H_2SO_4)(H_2O)_n$ and $(H_2SO_4)(NH_3)(H_2O)_n$ clusters with $n$ up to 50, it was established that the Rayleigh scattering only depends slightly on cluster morphology, and thereby identified minimum cluster structures will dominate the scattering properties. It was found that the Rayleigh scattering activity depends quadratically on the water content and that a single ammonia molecule is able to induce a high anisotropy in the particle. The hyper Rayleigh scattering intensities (*i.e* the elastic scattering of two incident photons into one with twice the frequency) was found to be very weak. Very recently, Jiang et al. used this type of approach for studying the scattering properties of small $Cl^-(H_2O)_n$ clusters with $n = 1 - 6$[41].

Herein we wish to study the Rayleigh light scattering properties of $(H_2SO_4)_a(NH_3)_b$ and $(H_2SO_4)_a((CH_3)_2NH)_b$ molecular clusters. As also indicated by their participation in nucleation, molecular clusters consisting of sulfuric acid and bases are known to exhibit strong intermolecular interactions, which will significantly increase the residence time of the clusters in the atmosphere. We will for the first time utilize these clusters and investigate optical properties of molecular clusters ranging up to nanometer sizes.

## 2 - Theory

### 2.1 - Rayleigh Scattering

The Rayleigh light scattering activities of the parallel ($\mathfrak{R}_{p\parallel}$), perpendicular ($\mathfrak{R}_{p\perp}$) components of the linearly polarized light and natural light ($\mathfrak{R}_n$) can be calculated as the following[42]:

$$\mathfrak{R}_n = 45(\bar{\alpha})^2 + 13(\Delta\alpha)^2 \tag{1}$$
$$\mathfrak{R}_{p\perp} = 45(\bar{\alpha})^2 + 7(\Delta\alpha)^2 \tag{2}$$
$$\mathfrak{R}_{p\parallel} = 6(\Delta\alpha)^2 \tag{3}$$

Here ($\bar{\alpha}$) and ($\Delta\alpha$) are the isotropic mean and anisotropic polarizabilities, respectively, which are given by:

$$\bar{\alpha} = \frac{1}{3}\sum_i \alpha_{ii} \tag{4}$$
$$\Delta\alpha = \sqrt{\frac{\sum_{ij}(3\alpha_{ij}\alpha_{ij} - \alpha_{ii}\alpha_{jj})}{2}} \tag{5}$$

In measurement of scattered light the depolarization ratio ($\rho$) is an important parameter. For Rayleigh scattering, the depolarization ratio of natural light $\rho_n$, plane-polarized light $\rho_p$ and circularly polarized light $\rho_c$ are given by:

$$\rho_n = \frac{6(\Delta\alpha)^2}{45(\bar{\alpha})^2 + 7(\Delta\alpha)^2} \tag{6}$$
$$\rho_p = \frac{3(\Delta\alpha)^2}{45(\bar{\alpha})^2 + 4(\Delta\alpha)^2} \tag{7}$$
$$\rho_c = \frac{\rho_n}{1 - \rho_n} \tag{8}$$

The depolarization ratio thereby indicates the degree of anisotropy in the system. For calculating the Rayleigh scattering intensities and depolarization ratios, the frequency dependent polarizabilities are required. These are obtained using linear response theory methods, and the linear response function can be expressed as[43]:

$$\langle\langle\hat{A};\hat{V}^\omega\rangle\rangle_\omega = \frac{1}{\hbar}\sum_{n\neq 0}\left[\frac{\langle 0|\hat{A}|n\rangle\langle n|\hat{V}^\omega|0\rangle}{\omega_{n0} - \omega} + \frac{\langle 0|\hat{V}^\omega|n\rangle\langle n|\hat{A}|0\rangle}{\omega_{n0} + \omega}\right] \tag{9}$$

From the linear response function the frequency dependent polarizability can be obtained by: $\alpha_{\alpha\beta}(-\omega;\omega) = -\langle\langle\mu_\alpha;\mu_\beta\rangle\rangle_\omega$. Here $\mu_\alpha$ and $\mu_\beta$ refer to dipole moment operators. The special case of $\alpha_{\alpha\beta}(0;0)$ correspond to the polarizability in the static limit. To analyse the change in scattering properties upon forming a cluster, the binding mean isotropic and anisotropic polarizabilities are defined as the following:

$$\bar{\alpha}_{\text{Binding}} = \bar{\alpha}_{\text{Cluster}} - \sum_i \bar{\alpha}_{\text{Monomer},i} \tag{10}$$
$$\Delta\alpha_{\text{Binding}} = \Delta\alpha_{\text{Cluster}} - \sum_i \Delta\alpha_{\text{Monomer},i} \tag{11}$$

### 2.2 - Cluster Dynamics

To obtain an indication of the steady state concentrations of different molecular clusters, we employ the Atmospheric Cluster Dynamics Code (ACDC)[44–46]. In the ACDC code the time derivatives of the concentrations of all clusters, also known as the birth-death equations, are solved. The time derivatives includes collision terms from smaller clusters and evaporation terms from larger clusters and the time derivative of the concentration for each cluster can be expressed as[44]:

$$\frac{dc_i}{dt} = \frac{1}{2}\sum_{j<i}\beta_{j,(i-j)}c_jc_{i-j} + \sum_j\gamma_{(i+j)\to i,j}c_{i+j}$$
$$- \sum_j\beta_{i,j}c_ic_j - \frac{1}{2}\sum_{j<i}\gamma_{i\to j,(i-j)} \tag{12}$$

here $c_i$ denotes the concentration of cluster $i$, $\beta_{i,j}$ is the collision coefficient of clusters $i$ and $j$, and $\gamma_{k\to i,j}$ is the evaporation

coefficient of cluster $k$ into clusters $i$ and $j$. Collision coefficients are obtained from kinetic gas theory[44]:

$$\beta_{i,j} = \left(\frac{3}{4\pi}\right)^{1/6}\left[6k_BT\left(\frac{1}{m_i} + \frac{1}{m_j}\right)\right]^{1/2}\left(V_i^{1/3} + V_j^{1/3}\right)^2 \quad (13)$$

where $m_i$ and $V_i$ are the mass and mass volume of cluster $i$, respectively. The evaporation rates are obtained from quantum chemical Gibbs free energy calculations as the following[45]:

$$\gamma_{(i,j)\to i,j} = \beta_{i,j}\frac{P_{\text{ref}}}{k_BT}\exp\left(\frac{\Delta G_{i+j} - \Delta G_i - \Delta G_j}{k_BT}\right) \quad (14)$$

where $\Delta G_i$ is the free energy of the formation of the cluster $i$ calculated at the reference pressure $P_{\text{ref}}$. Using these expressions, the steady state cluster distributions can be obtained.

## 3 - Computational Methodology

All calculations have been performed using the Gaussian09 program package[47]. We previously identified that the scattering properties were only negligible dependent on the cluster morphology, which indicates that minimum energy structures can be utilized[40]. Recently, large discrepancies were pointed out between the reported free energy values identified at the B3RICC2[45] and PW91/6-311++G(3df,3pd) level of theory concerning the formation of clusters involving dimethylamine[48]. We thereby re-evaluate the potential free energy surface of the studied clusters, prior to calculating the optical properties. The $(H_2SO_4)_a(NH_3)_b$ and $(H_2SO_4)_a((CH_3)_2NH)_b$ minimum structures with $a, b \leq 4$, are extracted from the publication by Ortega et al[45]. In our recent investigation, it became evident that multiple functionals should always be used when evaluating cluster formation free energies, since each functional was found prone to errors in individual and non-systematic ways[49]. On the basis of recent benchmarks[50–54], the PW91, M06-2X and $\omega$B97X-D functionals were chosen. The potential energy surface of the extracted structures with $a, b \leq 4$ have been re-calculated using the PW91/6-311++G(3df,3pd)//PW91/6-31++G(d,p), M06-2X/6-311++G(3df,3pd)//M06-2X/6-31++G(d,p) and $\omega$B97X-D/6-311++G(3df,3pd)//$\omega$B97X-D/6-31++G(d,p) level of theory. Reducing the basis set to 6-31++G(d,p) for obtaining the geometries and vibrational frequencies have been shown to only lead to small errors in the corresponding thermal contribution to the free energy[49]. To test the performance of the reduced basis set approach the clusters were also optimized at the M06-2X/6-311++G(3df,3pd) level of theory.

To model larger clusters with $a, b > 4$ a slightly different approach was used. These were obtained by adding acid-base pairs to the existing cluster structures and minimizing using an on the fly MMFF94 force field with a simulating annealing

approach while keeping the cluster as spherical as possible. Subsequently, a Born-Oppenheimer molecular dynamics simulation (BOMD) was performed at the semi-empirical PM6 level of theory. After a ~10 ps trajectory the cluster structure was extracted and further minimized at the PM6 level of theory to obtain the final structure. The frequency dependent and static polarizabilities are then subsequently calculated at the CAM-B3LYP/aug-cc-pvdz level of theory, which have previously been found sufficient accurate for modelling atmospheric molecular clusters[40]. All presented calculated optical properties are given in atomic units (a.u.). The conversion unit for the polarizability is 1 a.u. = 0.148 Å[3]

## 4 - Results and Discussion

### 4.1 - Evaluation of the Potential Energy Surface

The potential free energy surfaces have been evaluated for the studied clusters using four different levels of theory as mentioned in the previous section. In Table 1 the calculated binding free energy values of the $(H_2SO_4)_a(NH_3)_b$ clusters are presented.

| Cluster | PW91$_{\text{red}}$ | M06-2X$_{\text{red}}$ | $\omega$B97X-D$_{\text{red}}$ | M06-2X |
|---|---|---|---|---|
| $(H_2SO_4)_1(NH_3)_1$ | -7.51 | -6.72 | -6.05 | -7.43 |
| $(H_2SO_4)_1(NH_3)_2$ | -11.44 | -11.64 | -10.69 | -12.88 |
| $(H_2SO_4)_1(NH_3)_3$ | -10.66 | -8.37 | -9.57 | -9.03 |
| $(H_2SO_4)_1(NH_3)_4$ | -11.07 | -9.06 | -8.85 | -10.84 |
| $(H_2SO_4)_2(NH_3)_1$ | -19.33 | -21.43 | -20.56 | -20.87 |
| $(H_2SO_4)_2(NH_3)_2$ | -27.58 | -26.16 | -27.28 | -27.16 |
| $(H_2SO_4)_2(NH_3)_3$ | -29.81 | -30.50 | -30.88 | -30.78 |
| $(H_2SO_4)_2(NH_3)_4$ | -31.54 | -31.57 | -33.03 | -32.01 |
| $(H_2SO_4)_3(NH_3)_1$ | -26.37 | -29.90 | -28.31 | -31.10 |
| $(H_2SO_4)_3(NH_3)_2$ | -39.05 | -41.17 | -42.44 | -42.66 |
| $(H_2SO_4)_3(NH_3)_3$ | -50.06 | -52.41 | -52.72 | -53.73 |
| $(H_2SO_4)_4(NH_3)_4$ | -54.29 | -54.40 | -56.52 | -55.82 |
| $(H_2SO_4)_4(NH_3)_1$ | -30.18 | -38.74 | -34.33 | -39.40 |
| $(H_2SO_4)_4(NH_3)_2$ | -45.32 | -52.51 | -50.78 | -53.10 |
| $(H_2SO_4)_4(NH_3)_3$ | -57.48 | -65.80 | -62.97 | -65.73 |
| $(H_2SO_4)_4(NH_3)_4$ | -69.34 | -74.08 | -73.84 | -75.89 |

**Table 1** Gibbs free binding energy of $(H_2SO_4)_a(NH_3)_b$ cluster formation in kcal/mol. The subscript red indicates that a reduced 6-31++G(d,p) basis set is used for obtaining the geometry and vibrational frequencies.

It is observed for the clusters with 1-2 sulfuric acid molecules, that all three DFT methods agree relatively well, with the maximum discrepancies around 2 kcal/mol in the binding free energies. As the number of acid molecules increases and the clusters become larger the discrepancies between the functionals increase substantially. The largest discrepancies are observed for the PW91 functional compared to M06-2X and $\omega$B97X-D with differences up 8.56 kcal/mol in case of the $(H_2SO_4)_4(NH_3)$ cluster. The M06-2X and $\omega$B97X-D functionals agree significantly better and are in most cases within

a few kcal/mol of each other. This further emphasize our previous finding that it is required to use multiple functionals when calculating cluster formation, as outliers might be present. In Table 2 the calculated binding free energy values of the $(H_2SO_4)_a((CH_3)_2NH)_b$ clusters are shown for the applied DFT functionals.

| Cluster | $PW91_{red}$ | $M06\text{-}2X_{red}$ | $\omega B97X\text{-}D_{red}$ | M06-2X |
|---|---|---|---|---|
| $(H_2SO_4)_1((CH_3)_2NH)_1$ | -11.71 | -10.62 | -13.10 | -11.42 |
| $(H_2SO_4)_1((CH_3)_2NH)_2$ | -15.89 | -14.80 | -14.97 | -14.43 |
| $(H_2SO_4)_1((CH_3)_2NH)_3$ | -14.58 | -17.49 | -17.65 | -17.66 |
| $(H_2SO_4)_1((CH_3)_2NH)_4$ | -15.19 | -16.78 | -18.95 | -15.99 |
| | | | | |
| $(H_2SO_4)_2((CH_3)_2NH)_1$ | -26.89 | -30.76 | -31.45 | -30.75 |
| $(H_2SO_4)_2((CH_3)_2NH)_2$ | -38.60 | -41.68 | -43.65 | -42.06 |
| $(H_2SO_4)_2((CH_3)_2NH)_3$ | -43.54 | -47.98 | -48.63 | -47.83 |
| $(H_2SO_4)_2((CH_3)_2NH)_4$ | -46.39 | -51.14 | -55.39 | -53.00 |
| | | | | |
| $(H_2SO_4)_3((CH_3)_2NH)_1$ | -33.74 | -42.63 | -41.14 | -42.98 |
| $(H_2SO_4)_3((CH_3)_2NH)_2$ | -44.05 | -57.47 | -54.21 | -57.94 |
| $(H_2SO_4)_3((CH_3)_2NH)_3$ | -63.82 | -73.15 | -75.63 | -74.37 |
| $(H_2SO_4)_4((CH_3)_2NH)_4$ | -72.90 | -82.66 | -85.63 | -82.93 |
| | | | | |
| $(H_2SO_4)_4((CH_3)_2NH)_1$ | -36.95 | -50.54 | -46.42 | -49.08 |
| $(H_2SO_4)_4((CH_3)_2NH)_2$ | -60.95 | -73.44 | -69.99 | -73.48 |
| $(H_2SO_4)_4((CH_3)_2NH)_3$ | -75.40 | -88.21 | -88.10 | -88.99 |
| $(H_2SO_4)_4((CH_3)_2NH)_4$ | -82.06 | -100.81 | -103.32 | -101.59 |

**Table 2** Gibbs free binding energy of $(H_2SO_4)_a((CH_3)_2NH)_b$ cluster formation in kcal/mol. The subscript red indicates that a reduced 6-31++G(d,p) basis set is used for obtaining the geometry and vibrational frequencies.

Similarly to the case of ammonia containing clusters there are several discrepancies between the calculated binding free energy values of the different functionals. The discrepancies are seen to become severe for larger clusters with a maximum difference of 21.26 kcal/mol between the PW91 and $\omega$B97X-D functionals in the case of the $(H_2SO_4)_4((CH_3)_2NH)_4$ cluster. This discrepancy is not caused by large differences in the molecular structure as exemplified in Figure 1. Similarly to the ammonia containing clusters it is observed that the PW91 functional shows the largest discrepancies compared to M06-2X and $\omega$B97X-D, with mean absolute differences of 7.62 and 7.96 kcal/mol, respectively. The M06-2X and $\omega$B97X-D functionals are in good agreement with each other having a mean absolute difference of only 2.06 kcal/mol. These discrepancies can be rationalized from the fact that the PW91 functional does not contain any HF-exchange and thereby lack the correct behaviour of the systems at long range. It is observed that the reduction of the basis set to 6-31++(d,p) utilized in geometry optimization and frequency calculation only has a limited effect on the binding free energies. The difference between the M06-2X/6-311++G(3df,3pd)//M06-2X/6-31++G(d,p) and M06-2X/6-311++G(3df,3pd) calculated binding free energies are in all cases seen to be lower than 2 kcal/mol with a mean absolute difference of 0.79 kcal/mol. Even though we observe large discrepancies between the different functionals

in modelling the formation free energies, conclusions based on the quantitative trends are still valid. For instance, for all cases we observe a significant stabilization of the molecular cluster by exchanging ammonia with amines which is in good agreement with previous studies [18].

From the calculated binding free energies, stability diagrams can be constructed, which allows the potential growth paths of the clusters to be analysed. In Figure 2 the stability diagram for cluster formation steps in the sulfuric acid - ammonia system is presented at the M06-2X/6-311++G(3df,3pd) level of theory. The color have been coded such that red pathways correspond to unfavourable routes, which are susceptible to evaporation. The value of 10 kcal/mol have been chosen such that red pathways have similar magnitude in the free energy as the sulfuric acid dimer, which is known to be prone to evaporation and cannot form particles on its own under typical atmospheric conditions. We recently formulated a rough estimate for cluster stability, where it was shown that a $\Delta G$-value of ~15 kcal/mol is required for condensation and evaporation to match at typical atmospheric conditions [55]. Thereby, pathways with a more favourable value than -15 kcal/mol are coloured green. The intermediate values of -10 to -15 kcal/mol are color coded with yellow. It is observed in the sulfuric acid - ammonia system, that the initial small clusters either have unfavourable or low stepwise free energy values. This indicates that sulfuric acid - ammonia clusters are not able to grow on their own, which is consistent with the conclusions of several previous studies. In Figure 3 the stability diagram for cluster formation steps in the sulfuric acid - dimethylamine system is presented using the same color coding as before.

In the case of the sulfuric acid - dimethylamine system it is observed that initially stable clusters are formed, which are subsequently able to grow through different growth paths. It is seen that stable $(H_2SO_4)_2((CH_3)_2NH)$ and $(H_2SO_4)_2((CH_3)_2NH)_2$ clusters are formed from the $(H_2SO_4)((CH_3)_2NH)$ cluster colliding with either $H_2SO_4$ or a $(H_2SO_4)((CH_3)_2NH)$ pair. The formation of these small stable clusters are in perfect agreement with the recent investigation of Kürten *et al.* [38]. The stable $(H_2SO_4)_3((CH_3)_2NH)_2$ cluster can either be formed from the $(H_2SO_4)_2((CH_3)_2NH)$ cluster through collision with a $(H_2SO_4)((CH_3)_2NH)$ pair or from the $(H_2SO_4)_2((CH_3)_2NH)_2$ cluster through collision with a sulfuric acid molecule. The further growth of the clusters are observed to form by addition of a sulfuric acid molecule, with subsequent addition of a dimethylamine or by
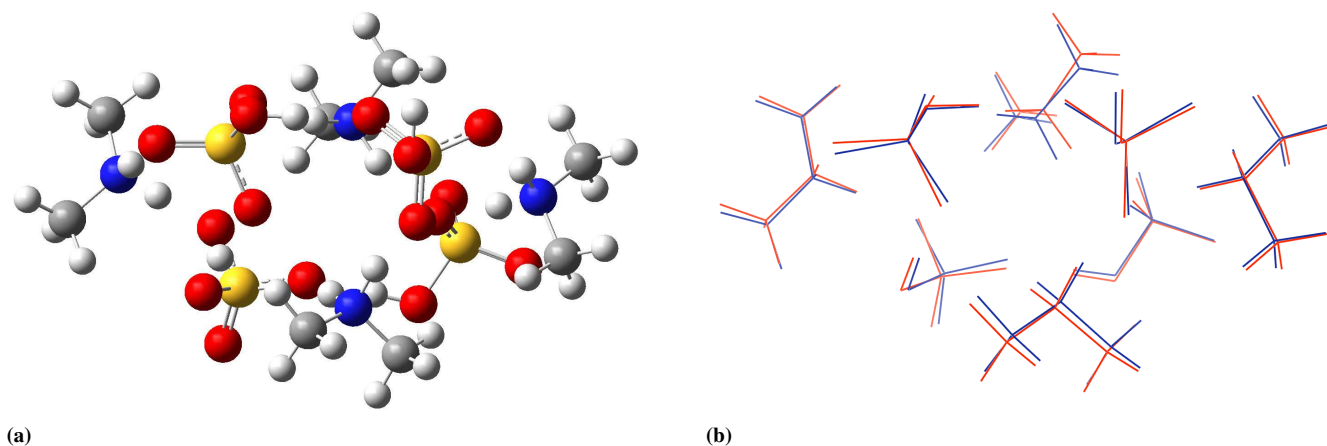
**Fig. 1** a) The $(H_2SO_4)_4((CH_3)_2NH)_4$ molecular cluster. b) The difference in molecular structure using the PW91 (red) or the $\omega$B97X-D (blue) functional.

(4sa)(1a)　　　　(4sa)(2a)

−8.30　−13.71

−14.57

(3sa)(1a)　−11.56　(3sa)(2a)　−10.45　(4sa)(2a)　−14.46

−10.23　　　　　　　−15.64

(2sa)(1a)　−6.29　(2sa)(2a)　−14.36　(3sa)(2a)　−11.07　(4sa)(3a)　−12.00　−20.07

−13.43　−12.29　−14.27　−15.50　−19.14　−22.95　−2.09　−14.73　−10.16

(1sa)(1a)　−5.45　(2sa)(2a)　−3.62　(3sa)(3a)　(3sa)(3a)　(4sa)(4a)

(1sa)(2a)　−10.46　(2sa)(3a)　−1.24　(3sa)(4a)　−23.81

+3.85　−21.74　−17.61

(1sa)(3a)　−15.55　(2sa)(4a)

−1.81　−21.17

(1sa)(4a)
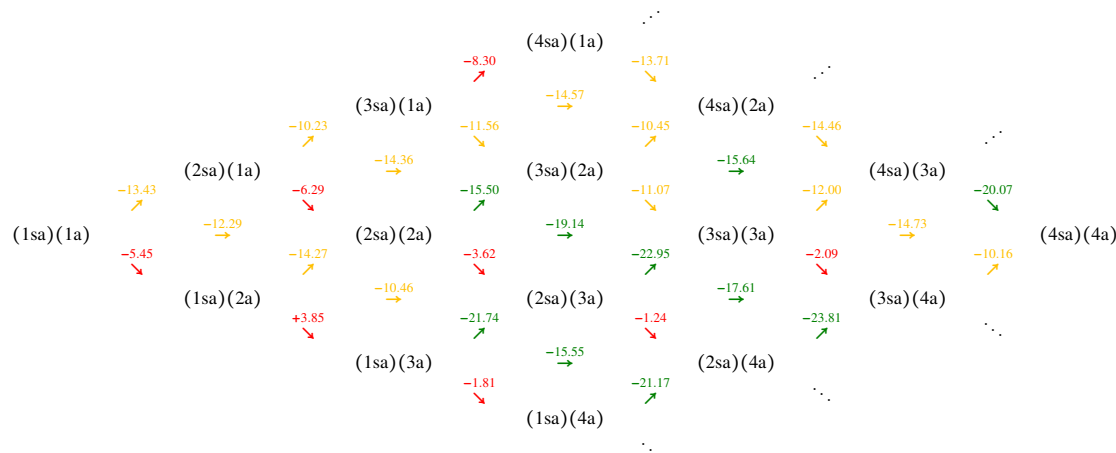
**Fig. 2** Stability diagram for cluster formation steps in the sulfuric acid (sa) - ammonia (a) system. The color is coded according to the Gibbs free energy of formation as follows: red, <10 kcal/mol; yellow, 10-15 kcal/mol and green, >15 kcal/mol. Values are reported at the M06-2X/6-311++G(3df,3pd) level of theory, at 298K.

collision with $(H_2SO_4)((CH_3)_2NH)$ pairs. This type of mechanism is in excellent agreement with the recent findings of Almeida *et al.* [37].

Using different functionals does in general produce very similar growth paths (See supporting information). In the case of the sulfuric acid ammonia system, all the functionals predict unfavourable formation of the initial clusters. For the sulfuric acid - dimethylamine system there is observed a few outliers. For the $(H_2SO_4)_2((CH_3)_2NH)_2 + H_2SO_4 \rightleftharpoons (H_2SO_4)_3((CH_3)_2NH)_2$ cluster formation, the calculated free energies are -5.45, -10.56 and -15.79 kcal/mol for the PW91, $\omega$B97X-D and M06-2X functionals, respectively.

## 4.2 - Cluster Populations

To obtain an estimate of the concentration of the molecular clusters we utilize the Atmospheric Cluster Dynamics Code (ACDC). The identified potential free energy surfaces are plugged into the ACDC code which allows for the estimation of the various clusters populations. In Figure 4 the $(H_2SO_4)_a(NH_3)_b$ and $(H_2SO_4)_a((CH_3)_2NH)_b$ cluster distributions can be seen calculated using the M06-2X/6-311++G(3df,3pd) potential energy surface at 298K.

(Figure 3 — stability diagram, with the following labelled states and transition energies)

(4sa)(1dma)

−6.10 ↗    −24.41 ↓

(3sa)(1dma)    −19.08 →    (4sa)(2dma)

−12.23 ↗    −14.97 ↙    −15.54 ↗    −15.51 ↘

(2sa)(1dma)    −15.77 →    (3sa)(2dma)    −19.63 →    (4sa)(3dma)

−19.33 ↗    −11.31 ↙    −15.88 ↗    −16.43 ↘    −14.62 ↙    −18.67 →

(1sa)(1dma)    −19.21 →    (2sa)(2dma)    −20.89 →    (3sa)(3dma)    −15.80 →    (4sa)(4dma)

−3.01 ↓    −27.63 ↗    −5.78 ↓    −26.53 ↗    −8.56 ↓    −12.60 ↗

(1sa)(2dma)    −21.98 →    (2sa)(3dma)    −23.67 →    (3sa)(4dma)

−3.23 ↓    −30.18 ↗    −5.16 ↓    −29.93 ↗

(1sa)(3dma)    −23.92 →    (2sa)(4dma)

+1.66 ↓    −37.00 ↗

(1sa)(4dma)

**Fig. 3** Stability diagram for cluster formation steps in the sulfuric acid (sa) - dimethylamine (dma) system. The color is coded according to the Gibbs free energy of formation as follows: red, $<10$ kcal/mol; yellow, 10-15 kcal/mol and green, $>15$ kcal/mol. Values are reported at the M06-2X/6-311++G(3df,3pd) level of theory, at 298K.
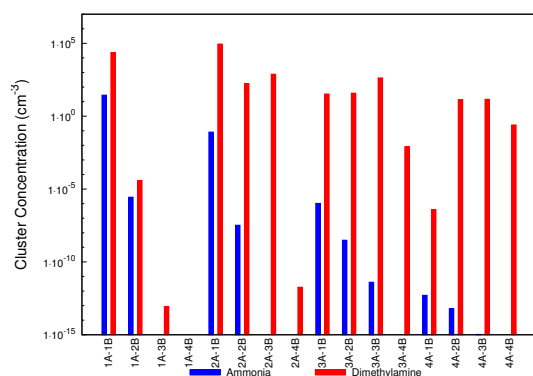
**Fig. 4** Steady state concentrations of $(H_2SO_4)_a(NH_3)_b$ (**blue**) and $(H_2SO_4)_a((CH_3)_2NH)_b$ (**red**) clusters. A and B refer to the number of Acids and Bases in the cluster, respectively.

It is seen that the concentrations fluctuate significantly, from cluster to cluster, with concentrations as low as $9 \cdot 10^{-30}$ cm$^{-3}$ for the $(H_2SO_4)(NH_3)_4$ cluster. The concentrations of the ammonia containing clusters are generally seen to be extremely low. The highest simulated concentration is observed to be 89,196 cm$^{-3}$ in the case of the $(H_2SO_4)_2((CH_3)_2NH)$ cluster. These simulated cluster concentrations are very dependent on the calculated binding free energies, and potential errors will resolve in errors of several orders of magnitude in the concentrations. For strongly bound clusters, there is also a competitive effect of growing out of the simulation box, leading to nucleating particles. In the case of the $(H_2SO_4)_a((CH_3)_2NH)_b$ clusters, the concentrations identified here are in good agree-

ment with the observed range of 100-100,000 cm$^{-3}$ of the background pool.

### 4.3 - Scattering Properties of $(H_2SO_4)_a(NH_3)_b$ and $(H_2SO_4)_a((CH_3)_2NH)_b$ Clusters, with $a,b \leq 4$

Based on the M06-2X/6-311++G(3df,3pd) re-optimized molecular clusters the Rayleigh light scattering intensities of natural light $(\mathfrak{R}_n)$ of the $(H_2SO_4)_a(NH_3)_b$ and $(H_2SO_4)_a((CH_3)_2NH)_b$ clusters, with $a,b \leq 4$ have been evaluated. In Figure 5 the calculated static (i.e. from $\alpha(0;0)$) Rayleigh light scattering intensities of natural light $(\mathfrak{R}_n)$ is presented as a function of cluster composition.
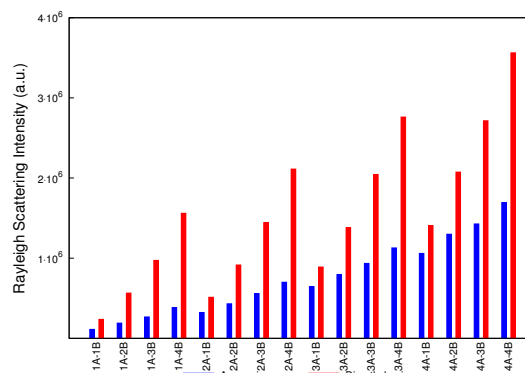
**Fig. 5** Rayleigh scattering intensities $(\mathfrak{R}_n)$ from $(H_2SO_4)_a(NH_3)_b$ (**blue**) and $(H_2SO_4)_a((CH_3)_2NH)_b$ (**red**) clusters. A and B refer to the number of Acids and Bases in the cluster, respectively.

It is observed that as the number of molecules increases in the cluster there is a rapid increase in the Rayleigh scattering intensity. Generally, we observe a significantly higher scattering from clusters containing amines than the corresponding ammonia containing clusters. This can be attributed by the significantly higher polarizability of 37.99 a.u. for dimethylamine compared to 13.91 a.u. for ammonia. For most of the clusters, we observe a slight decrease in the isotropic polarizability upon binding of up to 4.34 % in the case of the $(H_2SO_4)_4((CH_3)_2NH)_4$ cluster. We observe for the ammonia containing clusters a large anisotropic binding polarizability of 16-73% for all clusters except $(H_2SO_4)_4(NH_3)$. For the clusters containing amines we do not observe any definitive trends for the anisotropic binding polarizability. Half of the clusters have positive binding anisotropies, while the other half of the clusters have negative values. The depolarization ratios ($\rho_n$) are in general low for both types of clusters, ranging from 0.001 to 0.017. In most cases a substitution of an ammonia molecule with an amine will lead to a slight decrease in the depolarization ratio. This indicates that ammonia containing clusters are slightly more anisotropic than their amine containing counterparts.

The scattering properties are dependent of the wavelength of incident light. For each of the clusters the frequency dependent polarizability has been evaluated corresponding to wavelengths between 200 and 800 nm. When increasing the frequency of the light there is seen an increase in the Rayleigh scattering intensity. In Figure 6 this trend is exemplified with the $(H_2SO_4)(NH_3)$ cluster from 200 to 800 nm, in increments of 5 nm.
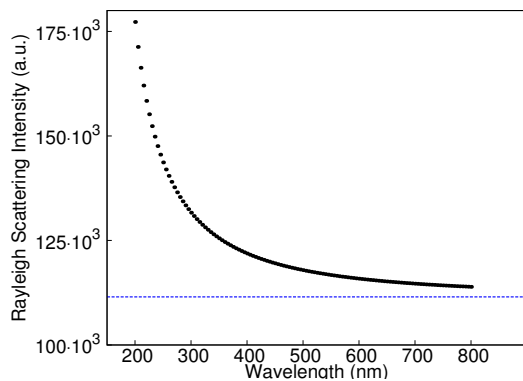


**Fig. 6** Dependence of the Rayleigh scattering intensities ($\mathfrak{R}_n$) on the wave length of the scattered light for the $(H_2SO_4)(NH_3)$ cluster. The blue line (- - -) corresponds to the static limit of the Rayleigh scattering intensity.

All clusters were observed to follow similar trends, but with varying slope of the curve. The ratio between the static Rayleigh scattering and the highest energy limit of 200 nm

$\left(\frac{\mathfrak{R}_n(200nm)}{\mathfrak{R}_n(\text{static})}\right)$ yield an indication about how the different clusters respond to the increase in the frequency of the light. In Table 3 the ratio can be seen for the $(H_2SO_4)_a(NH_3)_b$ clusters.

| a/sa | 1 | 2 | 3 | 4 |
|------|------|------|------|------|
| 1 | 1.59 | 1.45 | 1.43 | 1.41 |
| 2 | 1.78 | 1.50 | 1.45 | 1.44 |
| 3 | 1.80 | 1.56 | 1.47 | 1.43 |
| 4 | 1.98 | 1.64 | 1.52 | 1.47 |

**Table 3** Calculated ratio between the static Rayleigh scattering and the highest energy limit of 200 nm for $(H_2SO_4)_a(NH_3)_b$ clusters.

It is observed that keeping the number of sulfuric acid molecules fixed and increasing the amount of ammonia in the cluster will increase the response to the frequency of the light, leading to a larger ratio between the static and high frequency Rayleigh light scattering. The opposite trend is observed when keeping the amount of ammonia molecules fixed and increasing the number of sulfuric acid molecules in the cluster. The exact same trend is observed in the case of clusters consisting of dimethylamine.

As shown in section 4.1, the thermochemistry of ammonia and amine containing clusters shown in Figure 2 and 3 differs significantly. Above we have estimated the scattering properties of ammonia and amine containing clusters, but the concentration of the clusters in the atmosphere will also be directly relevant for the scattering properties. The effective Rayleigh scattering can thereby be expressed as:

$$\mathfrak{R}_{n,\text{eff}} = \mathfrak{R}_{n,i}c_i \qquad (15)$$

This yield the concentration dependent Rayleigh scattering of the different clusters. In Figure 7 the effective natural Rayleigh scattering, depending on concentration can be seen:
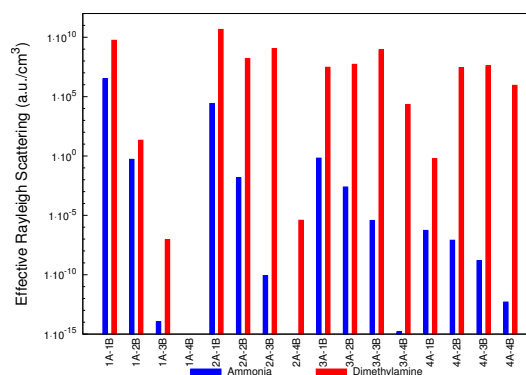


**Fig. 7** The effective natural Rayleigh scattering ($\mathfrak{R}_{n,\text{eff}}$) of $(H_2SO_4)_a(NH_3)_b$ (**blue**) and $(H_2SO_4)_a((CH_3)_2NH)_b$ (**red**) clusters. A and B refer to the number of Acids and Bases in the cluster, respectively.

It is seen that the Rayleigh scattering is very dependent on the distribution of the clusters. The highest observed effective scattering is seen from the $(H_2SO_4)_2((CH_3)_2NH)$ cluster with a value of $4.57 \cdot 10^{10}$ a.u./cm$^3$. For ammonia containing clusters the scattering is in all cases below 1, except for the $(H_2SO_4)(NH_3)$ and $(H_2SO_4)_2(NH_3)$ clusters with values of $3.12 \cdot 10^6$ a.u./cm$^3$ and $2.60 \cdot 10^4$ a.u./cm$^3$, respectively. These findings imply that the effective scattering of small atmospheric clusters are very dependent on the absolute concentration, and that there exists competitive pathways, such as nucleation and coagulation, which highly affects the ambient concentrations.

### 4.4 - Extension to Larger Clusters

From the stability diagrams in Figure 2 and 3 it is seen that the most stable clusters are those with an equal number of acids and bases. The clusters can thereby grow either by alternately adding one acid then one base molecule (and vice versa), or by addition of clusters containing acid-base pairs. To study larger clusters (i.e $a, b > 4$) we investigate how the scattering properties depend on the addition of equal amounts of acids and bases in the cluster ($a = b$). The Rayleigh light scattering properties of $(H_2SO_4)_a(NH_3)_b$ clusters with $(a = b) = 1\text{-}11$ have been investigated. These larger clusters were modelled using BOMD with the PM6 method as described in section 3. In Figure 8 the dependence of the Rayleigh light scattering intensity can be seen as a function of MD steps in the case of the $(H_2SO_4)_8(NH_3)_8$ cluster for a trajectory corresponding to 2.5 ps.
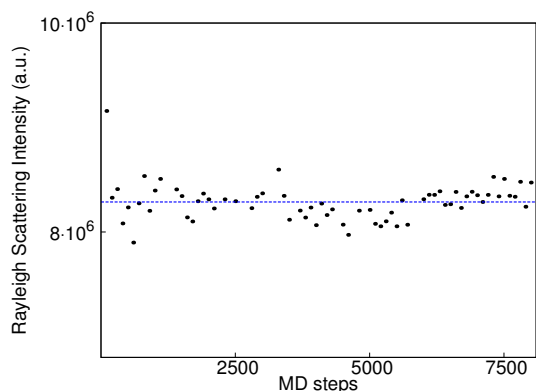


**Fig. 8** Rayleigh scattering intensities ($\mathfrak{R}_n$) as a function of MD steps for the $(H_2SO_4)_8(NH_3)_8$ cluster. The blue line (- - -) corresponds to the average of the scattering intensities *i.e.* 7,859,092 a.u.

It is observed that the Rayleigh scattering intensity is fluctuating more intensely in the beginning of the MD simulation, and quickly converges after roughly 0.5 ps, corresponding to 2000 MD steps. This behaviour have also been observed for other

electromagnetic properties[56]. The cluster structures with $a = b = 2 - 8$ have been recently been reported at the PW91/6-31++G(d,p) level of theory by Depalma et al.[12]. The Rayleigh scattering intensities ($\mathfrak{R}_n$) using the PW91/6-31++G(d,p) minimized $(H_2SO_4)_8(NH_3)_8$ cluster structure yield a value of 7,934,431 a.u. This value corresponds well with the range of $\mathfrak{R}_n$-values seen in Figure 8. Thereby, using this approach to yield the structure of larger clusters should be sufficiently accurate for the purpose of this study. Using the aug-cc-pVDZ basis set yielded severe convergence issues due to the inclusion of diffuse functions for cluster structures larger than 11 acid-base-pairs. The clusters were thereby evaluated using a small 6-31G(d) basis set for these clusters. Using the pople-style basis set yields significantly different polarizabilities. The ratio between the aug-cc-pVDZ and 6-31G(d) polarizabilities are found to vary from 1.55-1.75 for the $(H_2SO_4)_a(NH_3)_b$ clusters with ($a = b$) up to 11, with an average ratio of 1.63. This ratio is subsequently used to scale the 6-31G(d) results to yield a better indication of the correct scattering value. In Figure 9 the scattering properties of $(H_2SO_4)_a(NH_3)_b$ and $(H_2SO_4)_a((CH_3)_2NH)_b$ with ($a = b$) up to 20 can be seen as a function of acid-base pairs.
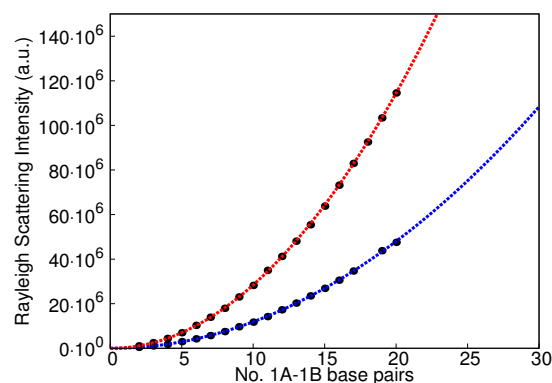


**Fig. 9** The Rayleigh scattering intensity ($\mathfrak{R}_n$) as a function of the number of acid-base pairs. The dotted lines corresponds to a quadratic fit to the calculated data points ●, with the blue line (- - -) for ammonia containing clusters and the red line (- - -) for amine containing. The Rayleigh scattering have been calculated using the 6-31G(d) basis set and scaled by a factor 1.63.

It is observed that as the number of acid-base pairs increases, the scattering intensity rapidly increase. The data points are seen to correlate well with a quadratic fit, illustrated by the red and blue dotted lines in Figure 9. This type of quadratic behaviour is to be expected from equation 1, since the ($\mathfrak{R}_n$)-value depends on the sum of the squared isotropic and anisotropic contributions. Due to the binding contribution to the polarizability, the exact form of the scattering is, however, not easily predicted without performing the actual calculation. It is

seen that the amine containing clusters scatter significantly more than the ammonia containing counterparts. This is similar to the behaviour of the smaller clusters and it is for instance seen that a $(H_2SO_4)_{20}((CH_3)_2NH)_{20}$ cluster scatters more than twice the amount as a $(H_2SO_4)_{20}(NH_3)_{20}$ cluster. The largest clusters investigated here are on the order of 1-2 nm and thereby corresponds well to a small nucleation mode particles. The observed large difference in the scattering by simply substituting ammonia with amines, further motivates the investigation of large clusters with compounds that exhibits large polarizabilities.

## 5 - Conclusions

We have investigated the Rayleigh light scattering properties of atmospheric molecular clusters consisting of $(H_2SO_4)_a(NH_3)_b$ and $(H_2SO_4)_a((CH_3)_2NH)_b$. The potential energy surfaces of clusters with $a, b \leq 4$ have been re-evaluated using four different levels of theory. It is found that using different DFT functionals can yield deviations of up to 21.26 kcal/mol in the binding free energies, as shown between the PW91 and $\omega$B97X-D functionals in the case of the $(H_2SO_4)_4((CH_3)_2NH)_4$ cluster. This indicates that more than one functional should be used when estimating the potential energy surface of atmospheric molecular clusters.

Using the ACDC code we estimate the cluster distributions from the identified potential energy surface at the M06-2X/6-311++G(3df,3pd) level of theory. Intrinsically, amine containing clusters scatter light more efficiently than their ammonia containing counterparts, but when taking the cluster concentrations into consideration a more complex behaviour is identified. There is a competitive pathway between nucleation and maintaining the background pool of atmospheric clusters, which highly affect the steady state concentrations.

Extending to larger particles with up to 20 acid-base pairs show a quadratic increase in the Rayleigh scattering. The quadratic behaviour of the Rayleigh light scattering intensity indicates that larger particles will scatter significantly more than small clusters. Contrarily, the smaller clusters might be present in larger concentrations. The effective scattering will thereby depend on both on the concentration and the size of the particle, and small atmospheric molecular clusters could potentially be important for the background scattering when present in large concentrations.

Since the effective Rayleigh scattering depends on the concentrations and clusters have the potential to subsequent nucleate and grow to larger sizes it is crucial to get a better understanding about the cluster distributions and scattering properties of clusters that exhibits weaker binding than amines. Oxidized organic compounds which show thermodynamically favourable interactions with sulfuric acid might be able to grow to larger sizes before they nucleate and thereby needs

to be further investigated. Furthermore, organic compounds might also influence the absorption properties, which might lead to a competing mechanism to Rayleigh scattering, dependent on the compound.

## References

1  J. Haywood and O. Boucher, *Rev. Geophys.*, 2000, **38**, 513–543.

2  M. Sipilä, K. Lehtipalo, M. Kulmala, T. Petäjä, H. Junninen, P. P. Aalto, H. E. Manninen, E. Kyrö, E. Asmi, I. Riipinen, J. Curtius, A. Kurten, S. Borrmann and C. D. O'Dowd, *Atmos. Chem. Phys.*, 2008, **8**, 4049–4060.

3  K. Lehtipalo, M. Sipilä, I. Riipinen, T. Nieminen and M. Kulmala, *Atmos. Chem. Phys.*, 2009, **9**, 4177–4184.

4  H. E. Manninen, T. Petaja, E. Asmi, I. Riipinen, T. Nieminen, J. Mikkila, U. Horrak, A. Mirme, S. Mirme, L. Laakso, V. M. Kerminen and M. Kulmala, *Boreal Env. Res.*, 2009, **14**, 591–605.

5  M. Kulmala, J. Kontkanen, H. Junninen, K. Lehtipalo, H. E. Manninen, T. Nieminen, T. Petj, M. Sipil, S. Schobesberger, P. Rantala, A. Franchin, T. Jokinen, E. Jrvinen, M. ijl, J. Kangasluoma, J. Hakala, P. P. Aalto, P. Paasonen, J. Mikkil, J. Vanhanen, J. Aalto, H. Hakola, U. Makkonen, T. Ruuskanen, R. L. Mauldin, J. Duplissy, H. Vehkamki, J. Bck, A. Kortelainen, I. Riipinen, T. Kurtn, M. V. Johnston, J. N. Smith, M. Ehn, T. F. Mentel, K. E. J. Lehtinen, A. Laaksonen, V.-M. Kerminen and D. R. Worsnop, *Science*, 2013, **339**, 943–946.

6  T. Kurtén, M. R. Sundberg, H. Vehkamäki, M. Noppel, J. Blomqvist and M. Kulmala, *J. Phys. Chem. A*, 2006, **110**, 7178–7188.

7  T. Kurtén, L. Torpo, M. R. Sundberg, V. Kerminen, H. Vehkamäki and M. Kulmala, *Atmos. Chem. Phys.*, 2007, **7**, 2765–2773.

8  T. Kurtén, L. Torpo, C. Ding, H. Vehkamäki, M. R. Sundberg, K. Laasonen and M. Kulmala, *J. Geophys. Res.*, 2007, **112**, D04210.

9  L. Torpo, T. Kurtén, H. Vehkamäki, K. Laasonen, M. R. Sundberg and M. Kulmala, *J. Phys. Chem. A*, 2007, **111**, 10671–10674.

10  J. Herb, A. B. Nadykto and F. Yu, *Chem. Phys. Lett.*, 2011, **518**, 7–14.

11  J. W. DePalma, B. R. Bzdek, D. J. Doren and M. V. Johnston, *J. Phys. Chem. A*, 2012, **116**, 1030–1040.

12  J. W. DePalma, D. J. Doren and M. V. Johnston, *J. Phys. Chem. A*, 2014, **118**, 5464–5473.

13  T. Kurtén, V. Loukonen, H. Vehkamäki and M. Kulmala, *Atmos. Chem. Phys.*, 2008, **8**, 4095–4103.

14  V. Loukonen, T. Kurtén, I. K. Ortega, H. Vehkamäki, A. A. H. Pádua, K. Sellegri and M. Kulmala, *Atmos. Chem. Phys.*, 2010, **10**, 4961–4974.

15  A. B. Nadykto, F. Yu, M. V. Jakovleva, J. Herb and Y. Xu, *Entropy*, 2011, **13**, 554–569.

16  P. Paasonen, T. Olenius, O. Kupiainen, T. Kurtén, T. Petäjä, W. Birmili, A. Hamed, M. Hu, L. G. Huey, C. Plass-Duelmer and et al, *Atmos. Chem. Phys.*, 2012, **12**, 9113–9133.

17  M. J. Ryding, K. Ruusuvuori, P. U. Andersson, A. S. Zatula, M. J. Mc-Grath, T. Kurtén, I. K. Ortega, H. Vehkamäki and E. Uggerud, *J. Phys. Chem. A*, 2012, **116**, 4902–4908.

18  O. Kupiainen, I. K. Ortega, T. Kurtén and H. Vehkamäki, *Atmos. Chem. Phys.*, 2012, **12**, 3591–3599.

19  D. J. Bustos, B. Temelso and G. C. Shields, *J. Phys. Chem. A*, 2014, **118**, 7430–7441.

20  A. B. Nadykto and F. Yu, *Chem. Phys. Lett.*, 2007, **435**, 14–18.

21  C. D. O'Dowd, P. Aalto, K. Hmeri, M. Kulmala and T. Hoffmann, *Nature*, 2002, **416**, 497–498.

22  R. Zhang, I. Suh, J. Zhao, D. Zhang, E. C. Fortner, X. Tie, L. T. Molina and M. J. Molina, *Science*, 2004, **304**, 1487–1490.

23  M. Sloth, M. Bilde and K. V. Mikkelsen, *Mol. Phys.*, 2005, **102**, 2361–2368.

24  H. Falsig, A. Gross, J. Kongsted, A. Osted, M. Sloth, K. V. Mikkelsen and O. Christiansen, *J. Phys. Chem. A*, 2006, **110**, 660–670.

25  Y. Xu, A. B. Nadykto, F. Yu, L. Jiang and W. Wang, *J mol. Struc.-THEOCHEM*, 2010, **951**, 28–33.

26  Y. Xu, A. B. Nadykto, F. Yu, J. Herb and W. Wang, *J. Phys. Chem. A*, 2010, **114**, 387–396.

27  L. Wang, A. F. Khalizov, J. Zheng, W. Xu, Y. Ma, V. Lal, and R. Zhang, *NATURE GEOSCIENCE*, 2010, **3**, 238–242.

28  W. Xu and R. Zhang, *J. Phys. Chem. A*, 2012, **116**, 4539–4550.

29  K. H. Weber, F. J. Morales and F. Tao, *J. Phys. Chem. A*, 2012, **116**, 11601–11617.

30  R. Zhang, *Science*, 2010, **328**, 1366–1367.

31  R. Zhang, L. Wang, A. F. Khalizov, J. Zhao, J. Zheng, R. L. McGraw and L. T. Molina, *PNAS*, 2009, **106**, 17650–17654.

32  J. Zhao, A. Khalizov, R. Zhang and R. L. McGraw, *J. Phys. Chem. A*, 2009, **113**, 680–689.

33  W. Xu and R. Zhang, *J. Chem. Phys.*, 2013, **139**, 064312:1–11.

34  K. H. Weber, F. J. Morales and F. M. Tao, *J. Phys. Chem. A*, 2012, **116**, 11601–11617.

35  Y. Liu, H. Wen, T. Huang, X. Lin, Y. Gai, C. Hu, W. Zhang and W. Huang, *J. Phys. Chem. A*, 2014, **118**, 508–516.

36  Y. Zhu, Y. Liu, T. Huang, S. Jiang, K. Xu, H. Wen, W. Zhang and W. Huang, *J. Phys. Chem. A*, 2014, **118**, 7959–7974.

37  J. Almeida, S. Schobesberger, A. Kurten, I. K. Ortega, O. Kupiainen-Maatta, A. P. Praplan, A. Adamov, A. Amorim, F. Bianchi, M. Breiten-lechner and et al., *Nature*, 2013, **502**, 359–363.

38  A. Kürten, T. Jokinen, M. Simon, M. Sipil, N. Sarnela, H. Junni-nen, A. Adamov, J. Almeida, A. Amorim, F. Bianchi, M. Breiten-lechner, J. Dommen, N. M. Donahue, J. Duplissy, S. Ehrhart, R. C. Flagan, A. Franchin, J. Hakala, A. Hansel, M. Heinritzi, M. Hutterli, J. Kangasluoma, J. Kirkby, A. Laaksonen, K. Lehtipalo, M. Leiminger, V. Makhmutov, S. Mathot, A. Onnela, T. Petj, A. P. Praplan, F. Ric-cobono, M. P. Rissanen, L. Rondo, S. Schobesberger, J. H. Seinfeld, G. Steiner, A. Tom, J. Trstl, P. M. Winkler, C. Williamson, D. Wim-mer, P. Ye, U. Baltensperger, K. S. Carslaw, M. Kulmala, D. R. Worsnop and J. Curtius, *Proceedings of the National Academy of Sciences*, 2014, 10.1073/pnas.1404853111.

39  S. Schobesberger, H. Junninen, F. Bianchi, G. Lönn, M. Ehn, K. Lehti-palo, J. Dommen, S. Ehrhart, I. K. Ortega, A. Franchin and et al., *Proc. Natl. Acad. Sci. U.S.A.*, 2013, **110**, 17223–17228.

40  J. Elm, P. Norman, M. Bilde and K. V. Mikkelsen, *Phys. Chem. Chem. Phys.*, 2014, **16**, 10883–10890.

41  S. Jiang, T. Huang, Y. Liu, K. Xu, Y. Zhang, Y. Lv and W. Huang, *Phys. Chem. Chem. Phys.*, 2014, **16**, 19241–19249.

42  L. Barron, *Molecular Light Scattering and Optical Activity*, Cambridge University Press, 2004.

43  J. Olsen and P. Jørgensen, *J. Chem. Phys.*, 1985, **82**, 3235–3264.

44  M. J. McGrath, T. Olenius, I. K. Ortega, V. Loukonen, P. Paasonen, T. Kurtén, M. Kulmala and H. Vehkamäki, *Atmos. Chem. Phys.*, 2012, **12**, 2345–2355.

45  I. K. Ortega, O. Kupiainen, T. Kurtén, T. Olenius, O. Wilkman, M. J. McGrath, V. Loukonen and H. Vehkamäki, *Atmos. Chem. Phys.*, 2012, **12**, 225–235.

46  T. Olenius, O. Kupiainen-Määttä, I. K. Ortega, T. Kurtén and H. Vehkamäki, *J. Chem. Phys.*, 2013, **139**, doi: 10.1063/1.4819024.

47  *Gaussian 09, Revision B.01, M. J. Frisch, G. W. Trucks, H. B. Schlegel, G. E. Scuseria, M. A. Robb, J. R. Cheeseman, G. Scalmani, V. Barone, B. Mennucci, G. A. Petersson, et al., Gaussian, Inc., Wallingford CT, 2010.*

48  A. B. Nadykto, J. Herb, F. Yu and Y. Xu, *Chem. Phys. Lett.*, 2014, **609**, 42–49.

49  J. Elm and K. V. Mikkelsen, *Chem. Phys. Lett.*, 2014, **615**, 26–29.

50  J. Elm, M. Bilde and K. V. Mikkelsen, *J. Chem. Theory Comput.*, 2012, **8**, 2071–2077.

51  J. Elm, M. Bilde and K. V. Mikkelsen, *Phys. Chem. Chem. Phys.*, 2013, **15**, 16442–16445.

52  H. R. Leverentz, J. I. Siepmann, D. G. Truhlar, V. Loukonen and H. Vehkamäki, *J. Phys. Chem. A*, 2013, **117**, 3819–3825.

53  N. Bork, L. Du and H. G. Kjaergaard, *J. Phys. Chem. A*, 2014, **118**, 1384–1389.

54  N. Bork, L. Du, H. Reimen, T. Kurtén and H. G. Kjaergaard, *J. Phys. Chem. A*, 2014, **118**, 5316–5322.

55  J. Elm, T. Kurtén, M. Bilde and K. V. Mikkelsen, *J. Phys. Chem. A*, 2014, **118**, 7892–7900.

56  T. Nymand, P. Astrand and K. Mikkelsen, *J. Phys Chem. B.*, 1997, **101**, 4105–4110.